Hindawi Publishing Corporation
Advances in Materials Science and Engineering
Volume 2011, Article ID 137387, 7 pages
doi:10.1155/2011/137387

Research Article

γ' Precipitation and Growth Kinetics in Mechanically Alloyed Ni–Al

QingXin Tang, Shigeharu Ukai, Akinobu Minami, and Shigenari Hayashi

Materials Science and Engineering, Faculty of Engineering, Hokkaido University, N13, W-8, Kita-ku, Sapporo 060-8628, Japan

Correspondence should be addressed to Shigeharu Ukai, s-ukai@eng.hokudai.ac.jp

Received 27 March 2011; Accepted 13 May 2011

Academic Editor: Kin Ho Lo

The precipitation and growth kinetics of γ' precipitates, which are strengthening factors in Ni-base oxide dispersion strengthened (ODS) superalloys, were investigated. The cuboidal-type γ' precipitates are formed in conventional arc-melted Ni–Al alloys, whereas spherical-type precipitates are formed in the mechanically alloyed (MAed) specimens. The morphology is controlled by a lattice misfit between the γ' precipitates and the matrix at the aging temperature of 800°C. The growth kinetics of the γ' precipitates can be followed by Ostwald ripening. The Arrhenius plot yielded a lower activation energy for the solute atom diffusion in MAed specimens, which is attributed to their high dislocation density and nanosized grains.

1. Introduction

In jet engines and gas turbines, where Ni-base superalloys with single crystals are currently used extensively as the materials for blades, disks, and vanes, the inlet temperature exceeds 1600°C. Next-generation Ni-base superalloys are intensively being developed to improve thermal efficiency by increasing inlet temperature; an oxide dispersion strengthened (ODS) type of Ni-base superalloy could be candidate of such alloy. The strength of Ni-base ODS superalloys is affected by both dispersed oxide particles and γ' precipitates with an $L1_2$ ordered structure. The coarsening behavior of γ' precipitates in Ni-base superalloys on being subjected to high temperature has been extensively investigated [1, 2]. Kusabiraki et al. [3] reported that coarsening of γ' precipitates in Inconel X-750 follows Ostwald ripening, according to the Lifshitz-Slyozov-Wagner (LSW) theory [4], which describes that an increase in the radius of γ' precipitates is proportional to $t^{1/3}$ (where t is the time). However, for mechanically alloyed (MAed) Ni-base ODS superalloys, experimental information on γ' precipitate behavior is extremely limited [5]. In this study, the precipitation and growth kinetics of γ' precipitates were investigated for the Ni–15at%Al alloy, Ni–15at%Al–0.6at%Y_2O_3 alloy, and similar MA6000 fabricated by ourselves by mechanical alloying and arc-melting as a reference, focusing on the effects of MA and Y_2O_3 addition.

2. Experimental Procedures

The elemental powders in the size of about 100 μm were provided to make three kinds of target compositions: Ni–15at%Al, Ni–15at%Al–0.6at%Y_2O_3, and similar MA6000 (Ni–15 wt%Cr–1.95 wt%Mo–4.45 wt%Al–2.9 wt%Ti–4 wt%W–1.9 wt%Ta–1 wt%Y_2O_3). These powders were placed in a pot 45 cc in volume together with stearic acid under argon gas atmosphere in a glove box, and they were mechanically alloyed (MAed) by using a planetary-type ball mill (Fritsch P-6). The weight ratio of ball to powder was set to 10 : 1. The mechanical alloying was processed for 24 h. Subsequently, the MAed powders were sintered by hot-pressing (HP) at 1200°C for 3 h. For comparison, the Ni–15at%Al alloy was fabricated by arc-melting and was then heat-treated at 1200°C for 72 h for forming a solid solution. Here, as-MAed powders are referred to "MA," the subsequently hot-pressed alloys of MAed powders are referred to "MAHP," and the arc-melted alloys are referred to "arc."

In order to measure hardness changes due to γ' precipitation, MAed powders were enclosed in an ampoule under vacuum, and the Vickers hardness test was conducted after annealing at four different durations—3 min, 10 min, 60 min, and 72 h at 800°C. The particle size of the MAed powders was about 50 μm. Hence, the Vickers hardness

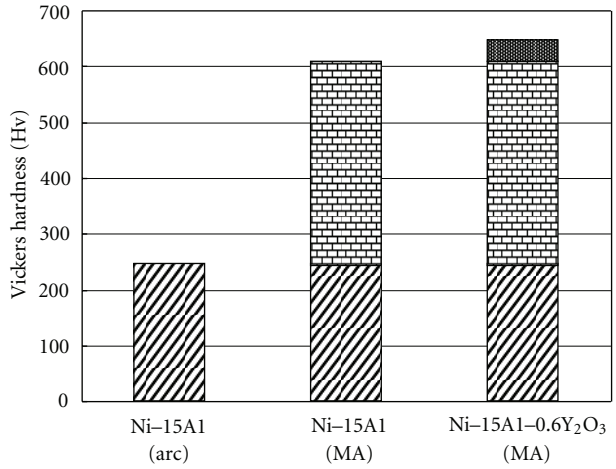

Figure 1: Vickers hardness at as-fabricated condition.

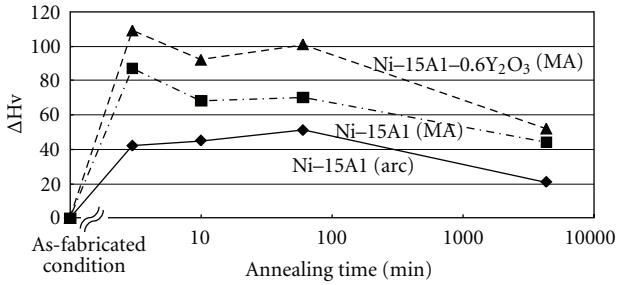

Figure 2: Hardness increase ΔHv during aging at 800°C.

measurement was carried out under lower loading of 100 gf for 5 s and was averaged for 10 times, with the maximum and minimum data points being neglected. For evaluating the growth kinetics of γ' precipitates, their scanning electron microscopy (SEM) observations were carried out after annealing for 24 h, 72 h, and 120 h at 800°C, 850°C, and 900°C.

3. Results and Discussion

3.1. Hardness Increase by γ' Precipitation. Figure 1 shows the results of hardness measurements under as-fabricated conditions of Ni–15at%Al (arc), Ni–15at%Al (MA), and Ni–15at%Al–0.6at%Y_2O_3 (MA). A comparison of the hardness values of the three kinds of alloys showed that mechanical alloying induces a hardness increase by Hv 350, which could be due to the introduction of severe plastic deformation during the alloying process. The addition of 0.6at%Y_2O_3 to Ni–15at%Al (MA) increases the hardness by approximately Hv 40.

The increase in hardness, ΔHv, from the hardness under the as-fabricated condition, induced by annealing at a temperature of 800°C is shown in Figure 2, where the annealing time is expressed in the logarithmic scale. Dislocation recovery and grain coarsening by annealing induce decrease in hardness. Results of X-ray diffraction analysis confirmed that this hardness increase is attributable to γ' precipitation during annealing, as shown in Figure 3, where the low-angle peak corresponds to the γ' precipitates and the high-angle one corresponds to the Ni solid solution in Ni–15at%Al (MA). The maximum ΔHv becomes Hv 50 for Ni–15at%Al (arc), Hv 90 for Ni–15at%Al (MA), and Hv 110 for Ni–15at%Al–0.6at%Y_2O_3 (MA). These results imply that the process of mechanical alloying leads to the hardness increase because of enhanced precipitation of γ'. With respect to Y_2O_3 behavior, it was found in a previous study that Y_2O_3 particles were dissociated by mechanical alloying, and then, yttrium and oxygen combined and reprecipitated as Y_2O_3 upon annealing at a temperature of around 600°C [6]. On the basis of these findings, it is concluded that Y_2O_3 particles do not directly affect the increase in hardness under the as-fabricated condition, as shown in Figure 1, and during annealing at 800°C, Y_2O_3 particles also precipitate and could affect the hardness increase of Ni–15at%Al–0.6at%Y_2O_3 (MA), as shown in Figure 2.

Table 1: Dislocation density and grain size of as-fabricated specimens produced by mechanical alloying and arc-melting.

	Dislocation density ($1/m^2$)	Grain size
Ni–15at%Al (MA)	3.65×10^{16}	91 nm
Ni–15at%Al–0.6at%Y_2O_3 (MA)	5.18×10^{16}	66 nm
Ni–15at%Al (arc)	8.50×10^{13}	3 mm

By X-ray diffraction analyses of the MAed powders and arc-melted alloy before annealing, the grain size (D) and accumulated strain (ε) were derived using the diffraction peak angle (θ) and width of the half height (β), according to (1) [7]

$$\beta \frac{\cos\theta}{\lambda} = 2\varepsilon \frac{\sin\theta}{\lambda} + \frac{K}{D}, \tag{1}$$

where λ is the wavelength of the incident X-ray (0.154 nm) and K is a constant (0.9). Furthermore, the dislocation density (ρ) can be estimated from accumulated strain (ε) using (2) [8]

$$\rho = 14.4 \frac{\varepsilon^2}{b^2}, \tag{2}$$

where b is the value of the Burgers vector (0.249 nm) in the Ni solid solution. Table 1 lists the analysis results. It is obvious that mechanical alloying results in extremely fine grains (grain size of the order of nanometers) and an extremely high dislocation density. These values are slightly enhanced by the addition of 0.6 at % Y_2O_3. Specimens produced by arc-melting have a large grain size of 3 mm and lower dislocation density. From the characterization of microstructures under the as-fabricated condition (Table 1), we find that the extremely fine grains and high dislocation density are responsible for the higher hardness in MAed and 0.6 at% Y_2O_3-added alloys.

3.2. γ' Precipitate Morphology. Figure 4 shows the SEM micrographs of Ni–15at%Al (MA) after annealing at 900°C

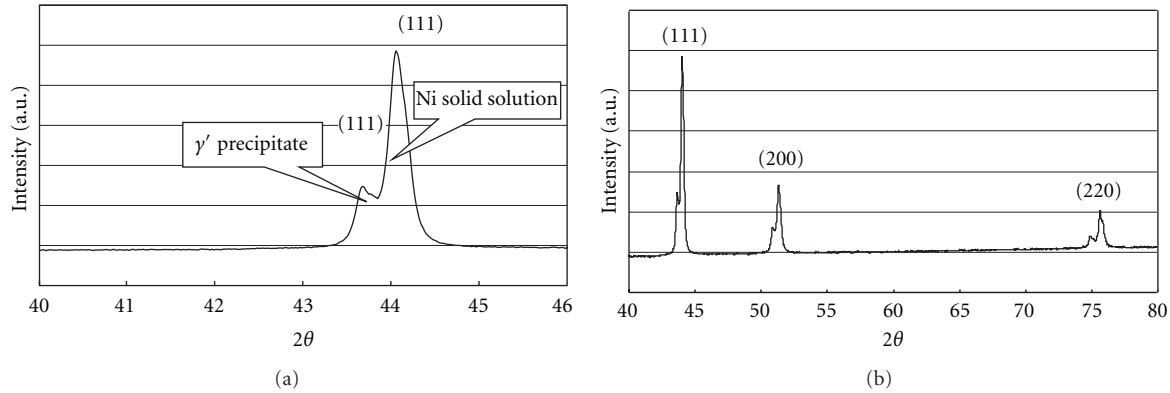

Figure 3: Results of X-ray diffraction for Ni-15at%Al (MA) after aging at 800°C.

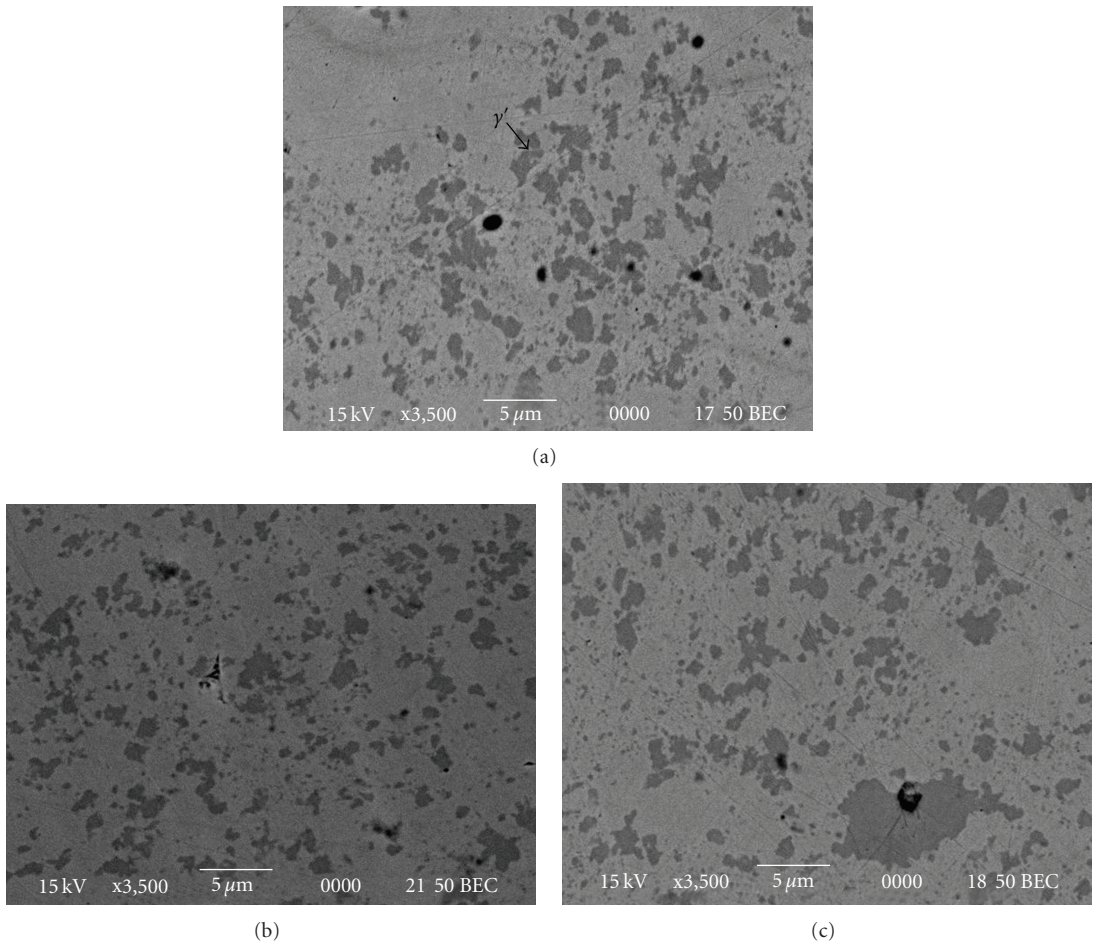

Figure 4: SEM micrographs of Ni-15at%Al (MA) after annealing at 900°C for 24 h (a), 72 h (b), and 120 h (c).

for 24 h, 72 h, and 120 h, and Figure 5 shows those of Ni–15at%Al (arc) under the same annealing conditions. The dark region corresponds to the γ' precipitates, which was confirmed by Ni and Al distributions by means of EPMA analyses. As shown in Figure 5, the γ' precipitates in dark region can be observed in regular arrangement along the lattice for arc-melted alloys. It was found that each array was composed of small cube type of γ' precipitates in a high magnification. A dimension of the cubes is approximately 0.3 μm (cuboidal morphology), and the cubes grow with increasing annealing duration. It is also reported by Ricks et al. [9] that the cube type of the γ' precipitates are developed on the (001) plane and coalescence into the cuboidal arrays. In contrast, the spherical-shaped γ' precipitates are

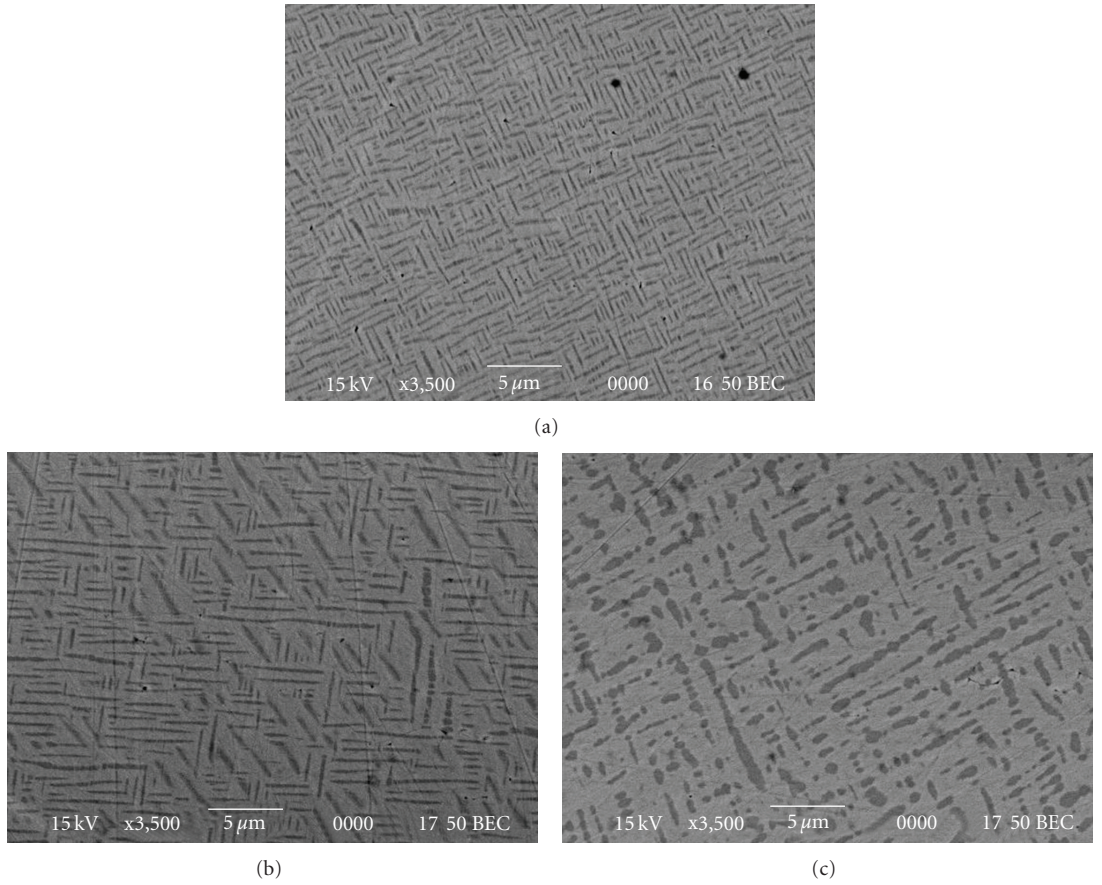

Figure 5: SEM micrographs of Ni-15at%Al(arc) after annealing at 900°C for 24 h (a), 72 h (b), and 120 h (c).

heterogeneously distributed in the MAed specimens, where each sphere appears to be an agglomeration of fine spheres in a dimension of approximately 0.2 μm. Figure 6 shows the distribution of γ' precipitates in the MAHP alloys of Ni–15at%Al, Ni–15at%Al–0.6at%Y_2O_3, and MA6000 after annealing at 900°C for 72 h. The γ' precipitates appear to be slightly arranged along a lattice, rather than spherical-type of agglomeration.

In order to evaluate the various morphologies of the γ' precipitates in MAed and arc-melted alloys, their lattice misfits were evaluated. On the basis of the X-ray diffraction measurements, the lattice constant a is calculated using

$$d = \frac{\lambda}{2\sin\theta}, \qquad a = d\sqrt{h^2 + k^2 + l^2}, \tag{3}$$

where θ is the diffraction angle, λ is the wavelength of the CuKα characteristic X-ray spectral line of 0.154 nm, and (h k l) is the index of the lattice plane. In the case of Ni–15at%Al (MA), the 2θ values of γ and γ' precipitates are 44.21° and 43.82°, respectively, as shown in Figure 3. The diffracted lattice plane is (111) for both cases. Substituting these values into (3), the lattice constant becomes $a_\gamma = 0.35441$ nm and $a_{\gamma'} = 0.35743$ nm. These lattice constants are at room temperature; the values at 800°C, where γ' precipitation occurs, must be calculated. The lattice constants of γ and γ' precipitates at 800°C are estimated to be $a_{\gamma\text{-}800} = 0.35928$ nm and $a_{\gamma'\text{-}800} = 0.36120$ nm by using thermal expansion coefficients of 1.279×10^{-5} (1/K) for γ and 1.320×10^{-5} (1/K) for γ' precipitates. The lattice misfit δ of Ni–15at%Al (MA) was found to be 0.54% at 800°C when these values were substituted into (4):

$$\delta = \frac{a_{\gamma'} - a_\gamma}{a_\gamma}. \tag{4}$$

The lattice misfit δ of Ni–15at%Al (arc) became 0.25% at 800°C when $2\theta = 43.69°$ for γ and $2\theta = 43.44°$ for γ' precipitates and $a_{\gamma\text{-}800} = 0.36333$ nm and $a_{\gamma'\text{-}800} = 0.36421$ nm. Similarly, the lattice misfit δ of Ni–15at%Al–0.6at%Y_2O_3 (MA) was found to be 0.61%. These results are listed in Table 2.

Table 2: Lattice misfit parameters at 800°C measured by X-ray diffraction.

	Lattice misfit (%)
Ni–15at%Al (MA)	0.54
Ni–15at%Al–0.6at%Y_2O_3 (MA)	0.61
Ni–15at%Al (arc)	0.25

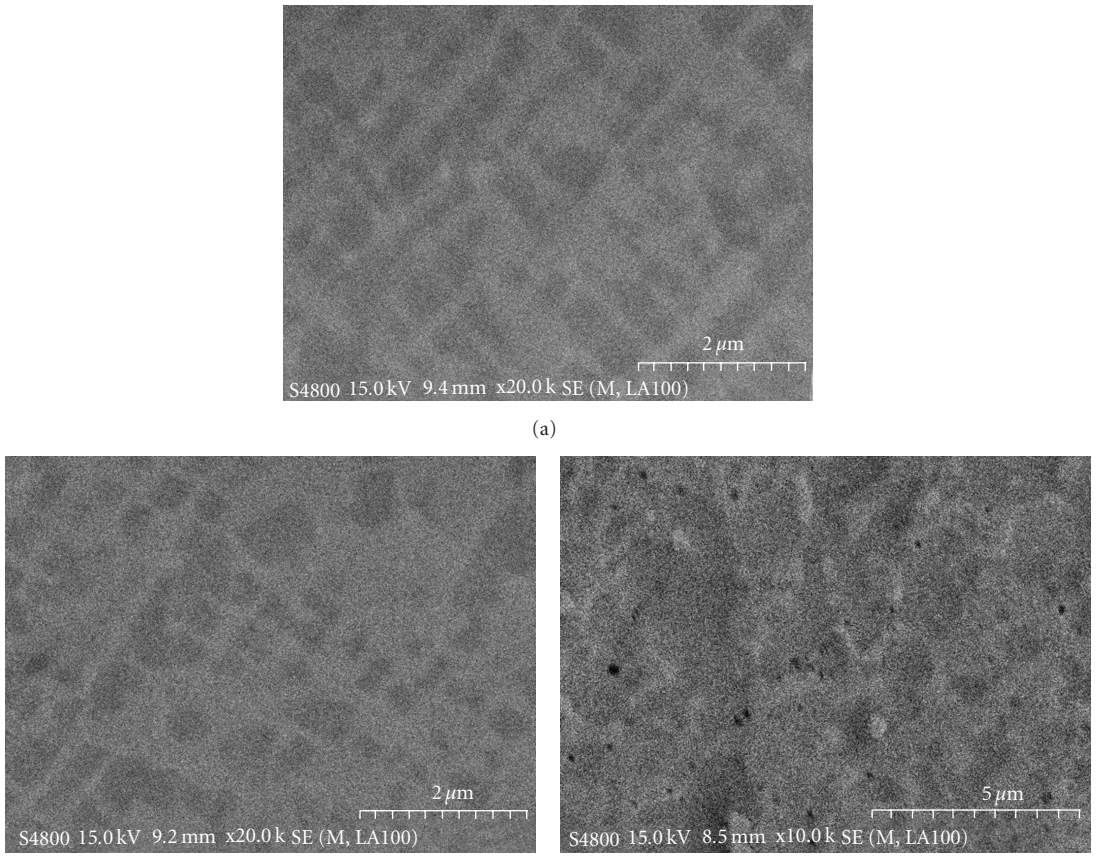

Figure 6: SEM micrographs for MAHP specimens after annealing at 900°C for 72 h. Ni-15at%Al (a), Ni-15at%Al-0.6at%Y_2O_3 (b), and MA6000 (c).

Table 3: The growth rate constant K′ (m^3/s) of γ' precipitates at 800°C, 850°C, and 900°C.

	800°C	850°C	900°C
Ni–15at%Al (arc)	4.20×10^{-27}	1.99×10^{-26}	9.22×10^{-26}
Ni–15at%Al (MA)	3.84×10^{-27}	6.84×10^{-27}	2.34×10^{-26}
Ni–15at%Al (MAHP)	3.91×10^{-26}	7.33×10^{-26}	1.23×10^{-25}
Ni–15at%Al–0.6at%Y_2O_3(MAHP)	7.94×10^{-26}	1.32×10^{-25}	1.81×10^{-25}
MA6000 (MAHP)	3.13×10^{-26}	5.87×10^{-25}	9.86×10^{-25}

If the lattice misfit δ between the γ and γ' precipitates is zero, γ' randomly precipitates in a spherical morphology; however, a slightly positive misfit results in a cuboidal γ' morphology, because preferential growth of the γ' precipitate occurs in the crystalline direction so as to minimize the elastic energy [9]. In addition, it has been reported that increasing the lattice misfit δ by more than 0.5% destroys coherency and leads to spherical precipitates [10]. The results listed in Table 2 are in agreement with the results mentioned above.

3.3. Growth Kinetics of γ' Precipitates. Figure 7 shows the sizes of the γ' precipitates for Ni–15at%Al (MA) with increasing aging time (24 h, 72 h, and 120 h) at 800°C, 850°C, and 900°C. The plot of the average size against the aging time is almost a straight line when the cube of the diameters of the γ' precipitates is considered although their individual sizes vary widely even at the same aging time and same temperature. This could imply that the growth of γ' precipitates is followed by Ostwald ripening, and the LSW relation would be satisfied, which is expressed as [11]

$$\overline{d^3} - \overline{d_0^3} = \frac{64\sigma D C_e V_m^2}{9RT} t = K' t,$$
$$K' = \frac{64\sigma D_0 C_e V_m^2}{9RT} \exp\left(-\frac{Q}{RT}\right), \tag{5}$$

where d_0 and d are average particle sizes at the initial time and after aging time t, σ is the interface energy between the γ' precipitate and the matrix, D is the diffusivity of the solute atom, C_e is the solute atom concentration in equilibrium with the γ' precipitate having infinite size, V_m is the molar volume of the γ' precipitate, R is the gas constant, and T is the absolute temperature. K' is the growth rate constant, which is expressed using the activation energy of atomic diffusion, Q. The value of K' at each temperature can be experimentally derived from the slope of the nominal values in Figure 8 although there is wide dispersion in upper and

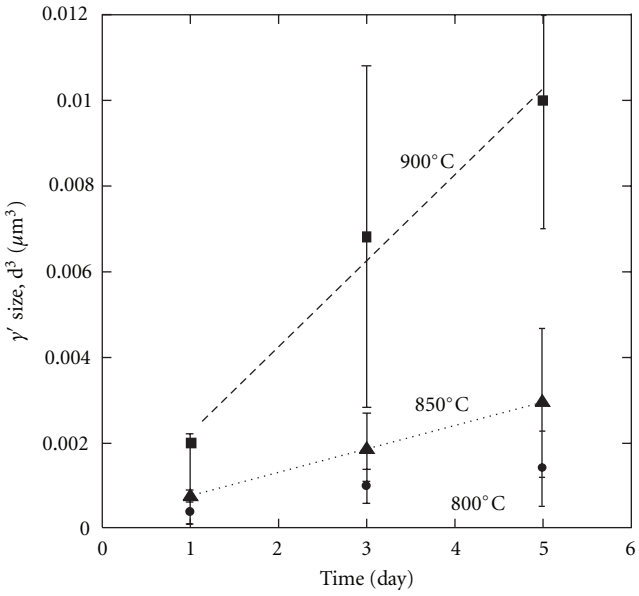

Figure 7: Cube of γ' precipitates size versus annealing time at 800°C, 850°C and 900°C for Ni-15at%Al (MA).

Table 4: Activation energy Q (kJ/mol) of atomic diffusion derived from growth rate of γ' precipitates.

	Activation energy of atomic diffusion (kJ/mol)
Ni–15at%Al (arc)	303
Ni–15at%Al (MA)	188
Ni–15at%Al (MAHP)	210
Ni–15at%Al–0.6at%Y_2O_3 (MAHP)	186
MA6000 (MAHP)	251

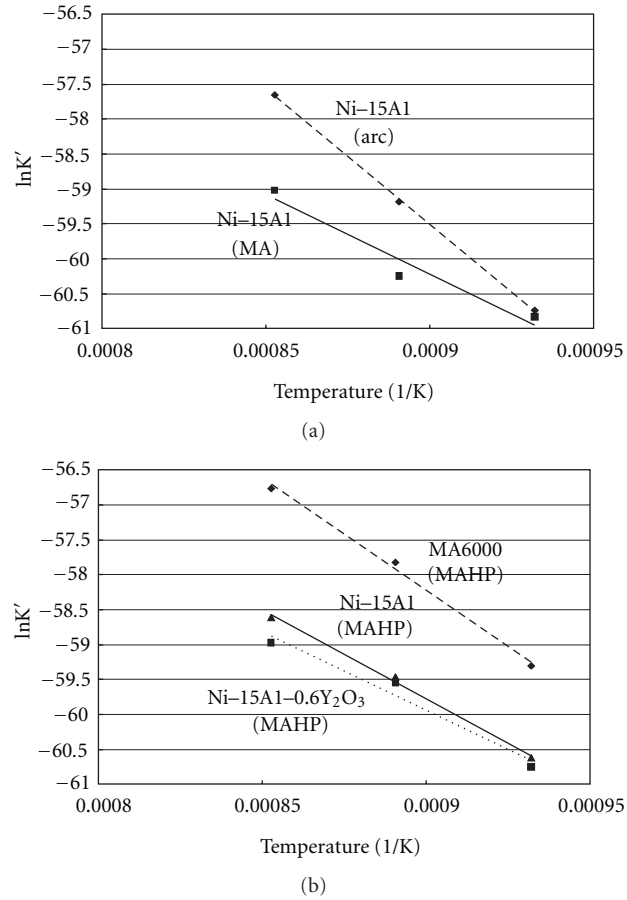

Figure 8: The Arrhenius plot for growth rate of γ' precipitates.

lower limits. Similarly, the values of K' were obtained for Ni–15at%Al (arc), Ni–15at%Al (MA and MAHP), Ni–15at%Al–0.6at%Y_2O_3 (MAHP), and MA6000 (MAHP); these values are listed in Table 3. They are represented by the Arrhenius plot of $\ln(K')$ versus $1/T$. The values of Q estimated from the slope of each line in Figure 8 are 188 kJ/mol for Ni–15at%Al (MA), 303 kJ/mol for Ni-15 at %Al (arc), 210 kJ/mol for Ni–15at%Al (MAHP), 186 kJ/mol for Ni–15at%Al–0.6at%Y_2O_3 (MAHP), and 251 kJ/mol for MA6000 (MAHP). These Q values are summarized in Table 4.

Kusabiraki et al. [3], Castani and Lupinc [12], Ardell and Nicholson [11, 13] pointed out that a growth of the γ' precipitates follows the LSW relation; the activation energy for the γ' growth is reported as 281 kJ/mol [3] and 290 kJ/mol [9] in Inconel X-750 and 269 kJ/mol [11] in Ni—Al. It is also pointed out that this activation energy belongs to that for diffusion of Al in Ni, of which activation energy is reported to be 268 kJ/mol [3]. In this study, similar activation energy of 303 kJ/mol was roughly estimated for the arc-melted alloys. However, MAed specimen is significantly reduced in the activation energy of 188 kJ/mol. This could be due to the high dislocation density and nanosized grains in MA, as shown in Table 1. It is considered that the atomic (Al) diffusion to produce γ' precipitates is adequately enhanced in MAed specimens. The activation energy for MAHP lies between that for MAed and that for arc-melted specimens and could be attributed to dislocation recovery and grain coarsening by hot-pressing at 1200°C for 3 h.

4. Conclusions

The γ' precipitation and growth kinetics in MAed Ni–Al specimens were investigated, and the following results were obtained.

(1) The morphology of the γ' precipitates is totally different: the morphology is cuboidal in the conventional arc-melted Ni—Al alloys and spherical in the MAed ones. These differences in morphologies are attributed to the different lattice misfits between the γ' precipitates and matrices at the aging temperature of 800°C. The arc-melted specimens have a lower positive value (less than 0.5%) of the lattice misfit δ, causing preferential growth of the γ' precipitate along the crystalline direction, whereas an increased lattice misfit δ (more than 0.5%) in the MAed specimen destroys coherency and leads to isotropic growth in spherical morphology.

The hardness increase induced by the γ' precipitates during aging is accelerated in the MAed specimens.

(2) The growth kinetics of the γ' precipitates can be expressed by Ostwald ripening. On the basis of the LSW theory, the activation energy for the γ' precipitate growth was derived from the Arrhenius plot: 303 kJ/mol for the arc-melted specimens, 188 kJ/mol for the MAed specimens, 210 kJ/mol for Ni–15at%Al (MAHP), 186 kJ/mol for Ni–15at%Al–0.6at%Y_2O_3 (MAHP), and 251 kJ/mol for the MAHP specimens. The lower activation energy for solute diffusion in the MAed specimen could be attributed to the high dislocation density and nanosized grains.

Acknowledgment

The authors are grateful to Tanikawa Fund Promotion of Thermal Technology for supporting this work.

References

[1] A. Maheshwari and A. J. Ardell, "Anomalous coarsening behavior of small volume fractions of Ni3Al precipitates in binary Ni–Al alloys," *Acta Metallurgica Et Materialia*, vol. 40, no. 10, pp. 2661–2667, 1992.

[2] A. K. Sinha and J. J. Moore, "Study of precipitation and growth of $\gamma\prime$ and dislocation structure in Inconel X-750," *Metallography*, vol. 19, no. 1, pp. 75–86, 1986.

[3] K. Kusabiraki, H. Nagahama, L. Wang, and T. Ooka, "Growth of $\gamma\prime$ precipitates in nickel-base superalloy," *Tetsu-To-Hagane*, vol. 75, no. 8, pp. 1354–1361, 1989 (Japanese).

[4] I. M. Lifshitz and V. V. Slyozov, "The kinetics of precipitation from supersaturated solid solutions," *Journal of Physics and Chemistry of Solids*, vol. 19, no. 1-2, pp. 35–50, 1961.

[5] HO. J. Ryu, S. H. Hong, J. Weber, and J. H. Tundermann, "Effect of elastic interaction energy on coarsening of $\gamma\prime$ precipitates in a mechanically alloyed ODS Ni-base superalloy," *Journal of Materials Science*, vol. 34, no. 2, pp. 329–336, 1999.

[6] T. Hoshino, S. Ukai, and S. Hayashi, in *Proceedings of the 5th ASM Heat Treatment and Surface Engineering Conference in Europe*, pp. 643–646, 2000.

[7] W. H. Hall, *The Journal of the Institute of Metals*, vol. 75, p. 1127, 1950.

[8] G. K. Williamson and R. E. Smallman, "III. Dislocation densities in some annealed and cold-worked metals from measurements on the X-ray debye-scherrer spectrum," *Philosophical Magazine*, vol. 1, pp. 34–46, 1956.

[9] R. A. Ricks, A. J. Porter, and R. C. Ecob, "The growth of $\gamma\prime$ precipitates in nickel-base superalloys," *Acta Metallurgica*, vol. 31, no. 1, pp. 43–53, 1983.

[10] R. C. Reed, *The Super Alloys, Fundamentals and Applications*, Cambridge University Press, Cambridge, UK, 2005.

[11] A. J. Ardell and R. B. Nicholson, "On the modulated structure of aged Ni-Al alloys. with an Appendix On the elastic interaction between inclusions by J. D. Eshelby Cavendish Laboratory, University of Cambridge, England," *Acta Metallurgica*, vol. 14, no. 10, pp. 1295–1309, 1966.

[12] C. Castani and V. Lupinc, "Solution heat treatment, aging and microstructure of inconel X-750," *Metallurgia Italiana*, vol. 69, no. 7-8, pp. 306–311, 1977.

[13] A. J. Ardell and R. B. Nicholson, "The coarsening of γ' in Ni-Al alloys," *Journal of Physics and Chemistry of Solids*, vol. 27, no. 11-12, pp. 1793–1794, 1966.